Journal of Materials Chemistry A

Large Area Multi-stacked Lithium-ion Batteries for Flexible and Rollable Applications

Journal:	*Journal of Materials Chemistry A*
Manuscript ID:	TA-ART-01-2014-000551.R1
Article Type:	Paper
Date Submitted by the Author:	21-Feb-2014

Complete List of Authors:	Kim, Joo-Seong; Korea Advanced Institute of Science and Technology, EEWS Lee, Yong-Hee; Korea Advanced Institute of Science and Technology, EEWS Lee, Inhwa; KAIST, Mechanical Engineering Kim, Taek-Soo; KAIST, Mechanical Engineering Ryou, Myung-Hyun; Hanbat National University, Choi, Jang Wook; Korea Advanced Institute of Science and Technology, EEWS

Journal of
Materials Chemistry A

RSCPublishing

PAPER

Large Area Multi-stacked Lithium-ion Batteries for Flexible and Rollable Applications†

Joo-Seong Kim[‡a], Yong-Hee Lee[‡a], Inhwa Lee[b], Taek-Soo Kim[b], Myung-Hyun Ryou[c]* and Jang Wook Choi[a]*

Cite this: DOI: 10.1039/x0xx00000x

Received 00th January 2014,
Accepted 00th January 2014

DOI: 10.1039/x0xx00000x

www.rsc.org/

The demand on flexible lithium ion batteries (LIBs) is successively increasing for timely advent of various flexible mobile electronic devices. Along this direction, a vast number of smart approaches such as implementation of conductive nanomaterials onto paper and textiles have been recently demonstrated. Most of them were, however, limited to single-cell levels. In the present study, in an attempt to expand the knowledge and design accumulated in the single-cell levels to larger-scale applications, large area flexible battery modules were developed. Multi-staking configuration was adopted for high areal energy density in each single-cell, while textile-based electrodes on both sides grant mechanical stability even in the module levels by efficiently releasing the stress generated during aggressive folding and rolling motions. Moreover, the connection and stacking of the single-cells give wide tuning capabilities in the overall voltage and capacity of the module. The current battery design should be immediately applicable to a broad range of outdoor, building, and military items.

Introduction

Lithium ion batteries (LIBs) have played a central role in wide propagation of mobile electronics into our everyday lives[1-5]. The successful fulfilment of LIBs as power sources has led to the birth of novel forms of portable electronic devices such as touch pads, e-book, and smart watches, and such trend of creating new conceptual devices and relevant markets is expected to continue. On the other hand, beyond simply serving as power supplies, LIBs are currently required to possess unconventional physical properties to keep pace with upcoming flexible and wearable electronic applications[6-11].

To meet this new demand, considerable research efforts have been invested to develop flexible and wearable LIBs based on new cell designs[12-16]. Along these directions, one of the most effective strategies is implementation of paper[17-19] and textiles[20, 21] as current collectors in lieu of conventional metal foil because inherent three-dimensional (3D) fibrous structures in paper and textiles can dissipate the stress generated during folding and bending motions of the battery assemblies. The intrinsic insulating nature of the paper and textiles were overcome by conformal coating of conductive carbon nanomaterials including carbon nanotubes[22-24] and graphene[25, 26] or traditional electroless metal deposition[27]. Other cell components, such as separator and electrode binder, which could affect successful achievement of such unconventional battery properties, have also been carefully investigated[28, 29].

Although the aforementioned demonstrations represent substantial progresses in the flexible/wearable battery research, most of the previous outcomes have been to the proof-of-concept levels limited to small areas within single-cell levels[30-32]. In the present study, having noticed such limited situation, we have expanded the textile batteries into large area multi-stacked platforms to cover emerging outdoor, building, and military applications. Detailed target items include tent, sleep bag, curtain/blind, curvy roof/eave, parasol, military jacket, military heating glove, multifunctional military goggles, etc. Moreover, the demonstrated module consisting of multiple single-cells is allowed to deliver wider ranges of the operation voltage and total capacity while maintaining bending and rolling capabilities, suggesting novel opportunities to tune the key battery parameters based on the cell design in both single-cell and module levels.

Experimental section

[a]*Graduate School of Energy, Environment, Water, and Sustainability (EEWS) and Center for Nature-inspired Technology (CNiT), KAIST Institute NanoCentury, 291 Daehakro, Yuseong-gu, Daejeon 305-701, Republic of Korea. E-mail: jangwookchoi@kaist.ac.kr*

[b]*Department of Mechanical Engineering, Korea Advanced Institute of Science and Technology (KAIST), 291 Daehakro, Yuseong-gu, Daejeon 305-701, Republic of Korea.*

[c]*Department of Chemical and Biological Engineering, Hanbat National University, Deokmyoung-dong, Yuseong-gu, Daejeon 305-719, Republic of Korea. E-mail: mhryou@hanbat.ac.kr*

† Electronic supplementary information (ESI) available: Fig. S1-S2, Video S1, S2.

‡ Equal contribution.

Electroless nickel deposition

The nickel (Ni)-coated loosely-woven and finely-woven textiles were prepared based on the commercial procedure reported previously[27]. Briefly, polyester fabric was dipped in 37% hydrochloric acid (HCl) solution containing 26 mM tin chloride ($SnCl_2$) for 10 min at 25 ºC for cleaning. For the textile activation, the samples were immersed in the solution containing 1.7 mM palladium chloride ($PdCl_2$), 37% HCl, and 0.32 M boric acid (H_3BO_3) at pH=2. Next, for electroless nickel deposition, the fabric samples were dipped into an aqueous solution containing 97 mM nickel sulfate ($NiSO_4$), 27 mM trisodium citrate dihydrate ($Na_3C_6H_5O_7 \cdot 2H_2O$), 0.34 M ammonium chloride (NH_4Cl), and 0.14 M sodium hypophosphite monohydrate ($NaH_2PO_2 \cdot H_2O$) for 30 min. Finally, the nickel-deposited fabric was washed with deionized water and dried at 150 °C for 20 min. The final Ni thickness was approximately 180-200 nm.

Synthesis of polyurethane binder

Polyurethane (PU) binder was synthesized according to the following procedure[27]: 4,4-diphenylmethane diisocyanate (MDI, 0.12 mmol), polytetramethylene glycol (PTMEG, 0.03 mmol), and polyethylene glycol (PEG, 0.03 mmol) were dissolved in 1 L of N,N-dimethylformamide (DMF), and then stirred for 5 h at 80 ºC to generate a well-mixed pre-polymer emulsion. Next, 0.06 mmol 1,4-butanediol was added to the pre-polymer emulsion, and the emulsion was then stirred again for 5 h at 80 ºC for further polymerization into the final polymer form. For use of PU as a binder, the final polymer emulsion was completely dried in a vacuum oven for 48 h at 70 ºC, and the dried polymer was dissolved again in N-methyl-2-pyrrolidone (NMP).

Characterization

Tensile tests were conducted to examine the stretchability of the Ni-coated textiles using a high-precision micromechanical test system (Delaminator Adhesion Test System; DTS Company, Menlo Park, CA, USA) with a customized jig. Various kinds of the textile electrodes and polymer films were cut into rectangular pieces with a length of 36 mm (or 21 mm only in the cases of PU films) and a width of 3 mm and were then stretched at a constant displacement rate of 20 μm s^{-1} until fracture of the specimens occurred. All of the fracture behaviours and electrical property changes during the pulling motions were recorded by an optical microscope (VHX-1000, Keyence, Osaka, Japan) and a multi-meter with four-point probes (Keithley 2000), respectively. Peel strength tests were also performed to measure the adhesion/cohesion strengths of the electrodes using the same micromechanical test system as the tensile tests. The specimen fabrication was conducted by cutting the electrode samples into the pieces with a size of 10 x 30 mm^2 (width x length), which were later attached to 3M tapes. By pulling the tapes at a constant displacement rate of 100 μm s^{-1}, the applied load was continuously monitored and the peel strength-displacement plots were attained. The Gurley number of the PU separator, defined as the time required for 100 cm^3 of air to pass through the membrane under an air pressure of 0.05 MPa, was out of the measurement range, indicating almost no porosity of the PU separator. But, the Li ionic conductivity was not hindered by good wettability of the PU separator through its hydrophilic domains as described previously[27].

Cell preparation

Active electrodes were prepared based on the following procedure: the active materials, denka black, and the PU binder solution were dispersed in NMP in a weight ratio of 80:10:10 for both cathodes and anodes. Commercial lithium iron phosphate ($LiFePO_4$ or LFP, Hanwha chemical) and lithium titanium oxide ($Li_4Ti_5O_{12}$ or LTO, POSCO ESM) were used as active materials of the cathodes and anodes, respectively. The well-mixed slurries were cast onto the Ni-coated polyester textiles by the doctor blade method. In each single-cell, the mass loadings of the active materials were 205 and 215 mg for the cathode (two layers) and anode (one layer), respectively, for an active area of 5 x 5 cm^2. The n/p ratio, defined as the actual anode capacity/the cathode capacity, was adjusted to 1.12 for the LTO/LFP full-cells. The electrochemical performances were characterized by preparing aluminum pouch full-cells (pouch size=10 x 11.5 cm^2). In these cells, PU separators (thickness=150 μm)[27] and 1 M lithium hexafluorophosphate ($LiPF_6$) dissolved in a mixture of ethylene carbonate (EC) and dimethyl carbonate (DMC) (EC/DMC=1:1=v/v, PANAX ETEC) were used as separators and electrolyte, respectively. The entire cell assembly was done in an argon-filled glovebox.

Electrochemical measurements

The electrochemical measurements were performed in the full-cell potential range of 0.6~2.4 V (single-cell) and 2.4~9.2 V (module) using a battery cycler (MACCOR series 4000). In each cycle, the charging and discharging processes were performed under CC & CV (limit current=0.1C) and CC modes, respectively. Also, in this study, the C-rate was defined based on the 1C value in each cell case, not actual charge/discharge durations. The electrochemical folding-unfolding tests were characterized by using a home-built linear stage machine (QS48, TPC motion).

Result and discussion

Fig. 1a shows how each single-cell obtains flexible and rollable capability. While each cell adopts the conventional stacking configuration in assembly of the electrodes and separator, the textile platforms in both electrodes distinguish the current single-cells from the conventional counterparts based on metal foil current collectors because 3D fiber networks inherently existing within the textiles can release the stress during folding and bending occasions and thus recover the original electrode structures persistently. In order to endow the conductivity with the given textile polyester in our case, Ni was coated on the textile by means of the established electroless deposition (see the Experimental section). A typical sheet resistance of the Ni-coated textile was ~0.35 Ω sq^{-1}, which is approximately 2~3 orders of magnitude lower than those based on the widely adopted dip coating of carbon nanomaterials. This far superior electronic conductivity is noticeable especially for the present large area cells because poor conductivity could restrict the increase in the cell area.

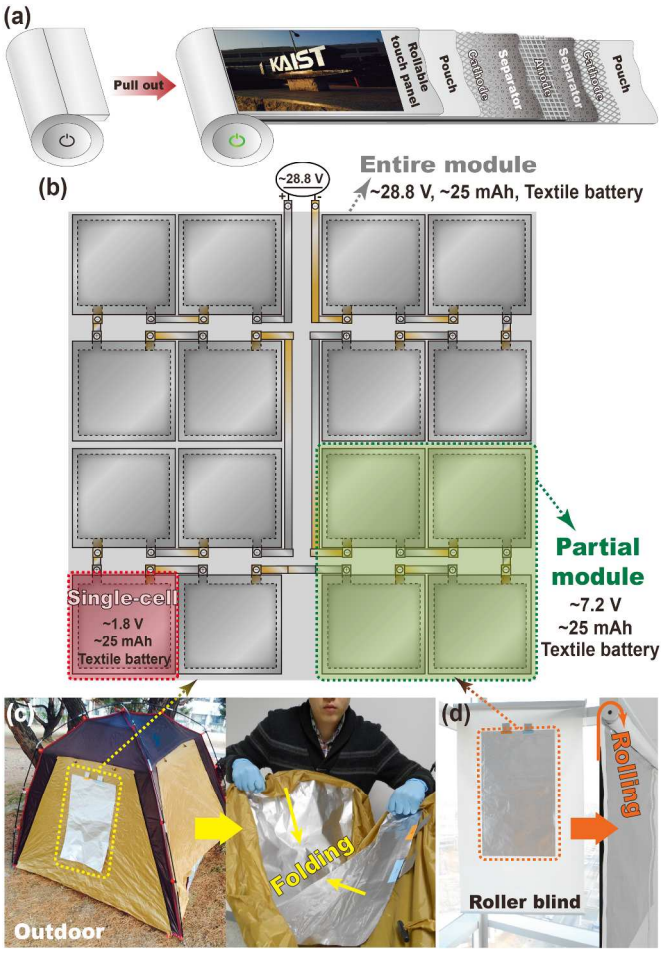

Fig. 1 (a) A schematic representation of a rollable display supported by a multi-stacked textile battery underneath. The detailed cell configuration consisting of the textile-based electrodes and PU separator is also presented. (b) A schematic illustration of the large area textile battery module. The single-cells with 1.8 V and 25 mAh are connected in series. The partial module (green area) consisting of 4 single-cells delivers 7.2 V and 25 mAh, and the entire module consisting of 16 single-cells delivers 28.8 V and 25 mAh. (c-d) Various potential applications based on large area multi-stacked Li-ion textile batteries. Photographs of multi-stacked textile batteries attached onto (c) an outdoor tent and (d) a roller blind beside a building window.

The connection of the single-cells gives additional degrees of freedom in the module design. For example, the connection in series could increase the operation voltage, whereas the connection in parallel could increase the overall capacity. Fig. 1b displays how 16 single-cells are connected in series to add up the voltage. Based on the active materials (LFP and LTO) chosen, each single-cell delivers 1.8 V, and the entire module consisting of 16 single-cells thus delivers 28.8 V. In addition, Fig. 1a, 1c, and 1d conceptually show representative items, namely electronic display, outdoor tent, and window blind, respectively, to which the current large area textile batteries are applicable. In the IT area, the flexible and foldable characteristics in the module level allow the current textile batteries to be integrated onto emerging flexible displays and could thus play a role in bringing the ubiquitous electronics to a reality. Similarly, for the outdoor tents, the textile batteries can be attached onto one of the curved tent sides and can thus be

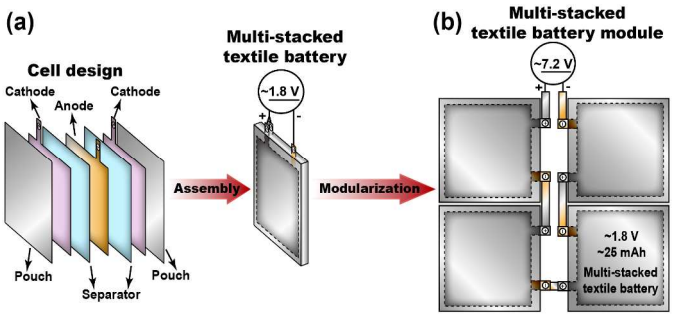

Fig. 2 Basic cell design. (a) In each single-cell, two sheets of the cathode sandwich a single sheet of the anode to increase the energy density at a given area. (b) A multi-stacked textile battery module. Each single-cell delivers 1.8 V and 25 mAh, and the module consisting of 4 single-cells based on the given connection delivers 7.2 V.

folded together when the main body of the tent is folded (Fig. 1c right). Also, the rollable characteristic of the textile battery module allows its entire body to follows the roller blind even when rolled into the roll at the end of the blind (Fig. 1d). These textile batteries could be combined with flexible solar cells in the purpose of efficient energy saving for buildings when installed in a way that the solar cells and textile batteries are attached on the opposite sides of the blind.

The application range of the current textile battery module could be varied depending on its energy density that is determined by the total capacity and operation voltage. One of the well-known strategies in increasing the total capacity is multi-stacking of the given electrodes. To adopt such multi-stacking approach, in the assembly of each single-cell, two sheets of the cathode textile were stacked on both sides of the anode textile with the separators sandwiched in between, as shown in Fig. 2a. Notably, the use of both sides of the anode textile was enabled by the 3D fibrous network structure in the anode textile that allows for Li-ion diffusion in both directions. Each single-cell delivers ~1.8 V based on the given pair of the electrodes, LFP and LTO, and ~25 mAh for the given area of 5 x 5 cm^2. This capacity value is indeed approximately doubled as compared to that based on the single-stack approach[27] employing the same cell preparation. The basic module in this study is composed of 4 double-stacked single-cells, and thus delivers 7.2 V, as displayed in Fig. 2b.

Flexible batteries should preserve electrochemical performance even during aggressive folding and bending motions. In particular, multi-stacking cells could experience enhanced strains from their greater thicknesses and should thus have better tolerance against such physical motions. In typical bending/folding motions, a different level of strain tends to be exerted onto each component layer across the cell stack, as depicted in Fig. 3a. For instance, in our case, when an aggressive folding was applied such that the folding angle reaches 160º, the outer and inner cathode layers are calculated to exercise 26% tensile and 19% compressional strains with respect to the middle anode layer, respectively (See Fig. S1†). In order to assess whether the Ni-coated textile can endure these tensile/compressional strains, the microstructure of the prepared Ni-coated textile was visualized during the given strain conditions (Fig. 3b). From these images, it was confirmed that the 3D porous network within the textile can afford to accommodate the given compressional/tensile strains by modifying the pore shapes. By contrast, conventional aluminium foil was ripped off even after a 1% tensile strain was

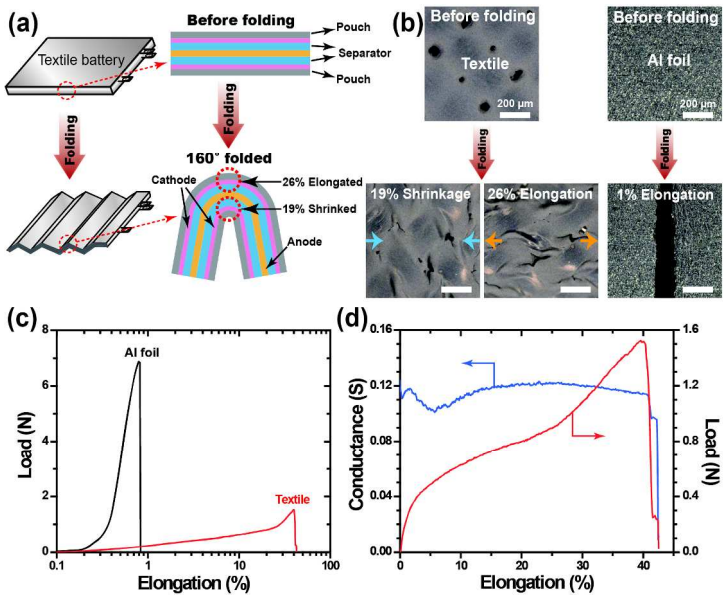

Fig. 3 Physical characterization of the Ni-coated textile. (a) A schematic illustration of compressional and tensile stress exerted onto the folding edge when the cell assembly was folded at multiple points as shown in the bottom left. Detailed dimensional change for each cell layer is denoted for the folding angle of 160º. (b) Comparative optical images of the textile-based and conventional foil-based current collectors during stretching/shrinking motions. The 3D porous structure of the textile accommodates the substantial tensile/compressional stress during stretching/shrinking motions, whereas the conventional aluminum foil rips off even after 1% elongation due to its rigid characteristic. (c) Tensile load-elongation curves for the aluminum foil and Ni-coated textile. (d) Conductance (blue) of the Ni-coated textile at different elongation ratios alongside the load (red) applied to the textile.

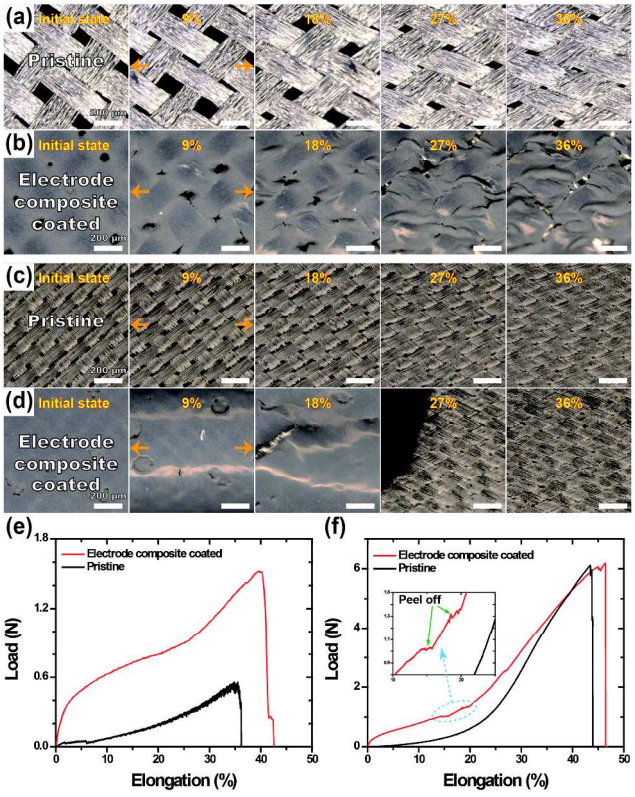

Fig. 4 The structures and mechanical properties of the Ni-coated textiles woven based on different methods. Optical images of the loosely-woven textile (a) without and (b) with the electrode composite coated at various elongation ratios. (c-d) The images based on the same measurements but for the finely-woven textile. The elongation rates were all 20 μm s^{-1}. Tensile load-elongation curves of the bare and electrode composite-coated textile for (e) the loosely-woven and (f) finely-woven cases.

applied (Fig. 3b right). The superior tolerance against the tensile motion was quantitatively verified in load-elongation curves (Fig. 3c). In the case of aluminum foil, the tensile stress generated turned out to be over six times as large as that of the Ni-coated textile, and the tensile tolerance was even less than 1% elongation, which is consistent with the optical microscope characterization in Fig. 3b. As shown in Fig. 3d, the film conductance of the Ni-coated textile remained preserved until the strain reached as high as 40%. After the elongation surpassed ~40%, the conductance dropped abruptly because the crossed yarns began to be untangled. The tolerance against compressional/tensile strains could be further enhanced if thinner textiles were chosen because the strain is directly related to the cell thickness as indicated by the equation in Fig. S1†.

The tolerance against various strains could also be varied depending on the weaving structure of the textile. In an attempt to see the weaving structure dependence, two types of the textile were tested: a loosely-woven one and a finely-woven one. For reference, the threads in the textile are divided into warp threads (vertically oriented) and weft threads (horizontally oriented), and the density of the threads in each orientation is described by the number of threads per inch: ends per inch (EPI) for warp and picks per inch (PPI) for weft. The EPI and PPI of the loosely-woven textile in our study were 110 and 92, respectively, whereas those of the finely-woven textiles were 260 and 190, indicating that the thread density of the finely-woven textile is about 2.21 times higher. Figs. 4a and b show optical microscope images at various elongation ratios from 0 to 36% for the loosely-woven textile without and with the LFP electrode components cast on top (5 mg cm^{-2}), respectively. Figs. 4c and d are the same cases but based on the finely-woven textile. These two different types of the textiles exhibited

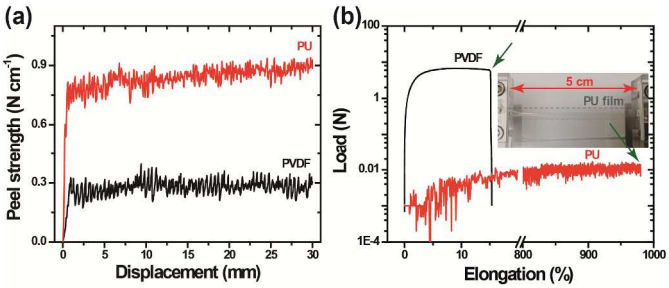

Fig. 5 Physical properties of the PU and PVDF binders. (a) Peel strengths of the battery composite electrodes containing both binders (LFP : denka black : binder = 80 : 10 : 10 in weight) when case onto Al foil. (b) Load-elongation curves of the PVDF and PU pure binder films (thickness ~50 μm for both cases). (Inset) a measurement apparatus for tensile stretching showing that the PU film was elongated more than 980%.

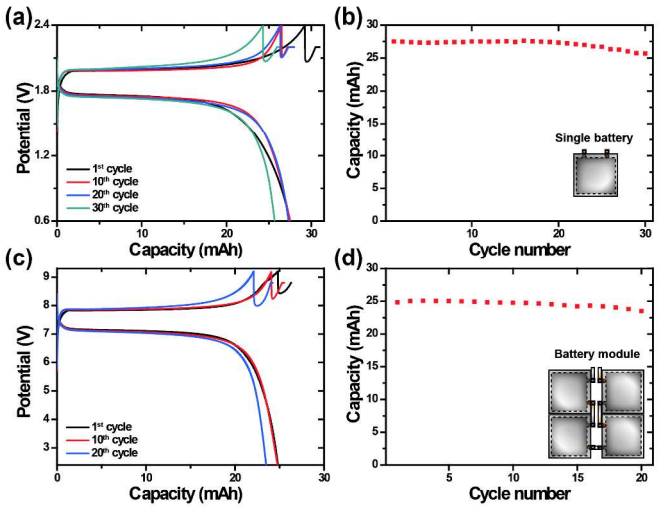

Fig. 6 Electrochemical characterization of multi-stacked textile batteries in single-cell and module levels. (a) Voltage profiles and (b) cycle life of the single-cell textile battery whose configuration is shown in Fig. 2a. Each single-cell delivers ~1.8 V and ~25 mAh. The C-rate for all of these results is 0.5C (=16.76 mA) for both charge and discharge in each cycle. (c) Voltage profiles and (d) cycle life of the multi-stacked textile battery module in which 4 single-cells are connected in series as shown in the inset schematic of (d). The C-rates for all of these results were 0.5C (=15.61 mA) for both charge and discharge in each cycle. All of the data in this figure were measured at room temperature.

conspicuously distinct behaviours in their tolerance against the elongation. In the case of the loosely-woven textile, the electrode film remained adhered all the way until 36% elongation, whereas the electrode film on the finely-woven textile peeled off after 18% elongation. In order to understand these distinctive behaviours, it is instructive to see how the textile releases the tensile stress. Upon tensile stretch, the textile releases the stress by aligning warp and weft threads in a direction where the angle between both threads decreases. In this angle adjustment process, the finely-woven textile generates higher stress, which could surpass the areal adhesion force of the electrode film. For this reason, the electrode film adhesion is more vulnerable for the case of the finely-woven textile. The microscopic structural changes shown in Figs. 4b and d were also recorded as video files (Video S1† and S2†, respectively) during continuous elongation.

Figs. 4e and 4f are the load vs. elongation curves for both types of the textiles. In both curves, it was observed that once the electrode films were coated on the textiles, the load values increased because the electrode films exert some stress against the tensile motions of the textiles. Furthermore, the curve in Fig. 4f shows load-lagging behaviors at multiple points during the elongation (Fig. 4f inset), which reflects the peel-off of the electrode film.

The distinct adhesion of the electrode film, in turn, signifies the crucial role of the polymeric binder in the electrode components. In the present investigation, a PU binder was employed instead of the conventional polyvinylidene fluoride (PVDF) binder. Fig. 5a exhibits the peeling strengths of both binder cases and reveals that the adhesion of the PU electrode film is 3~4 times stronger than that of the PVDF electrode counterpart. Furthermore, the results from the tensile stress tests of pure binder films showed totally distinguishing properties between both binders (Fig. 5b). The PVDF binder film fractured only after 15% elongation, whereas the PU binder film never fractured even at the elongation limit of the instrument, 980%. The exerted stress during the given tensile tests was also ~680 times smaller for the PU binder film. The superior adhesion and the more elastic nature of the PU binder indicate its suitable character for flexible batteries that are required to sustain during a variety of aggressive physical motions.

Electrochemical tests were conducted in both single-cell and module levels. The single-cell exhibited well-defined flat plateaus near 1.8 V (Fig. 6a). The flat plateaus at 1.8 V during full-cell discharge are reflective of the well-defined voltage profiles of both electrodes: 3.4 V vs. Li/Li^+ for LFP lithiation and 1.6 V vs. Li/Li^+ for LTO delithiation. The single-cell showed a capacity of 25 mAh for the cell area of 5 x 5 cm^2 and retained 93.4% of this initial capacity after 30 cycles (Fig. 6b), implying that the cell was well-prepared on the basis of the controlled n/p ratio (=1.12). In the case of a module consisting of 4 single-cells, the operation voltage around 7.2 V with well-defined plateaus was observed (Fig. 6c), verifying good connections among the highly functional single-cells. The module also showed robust cycling performance, as 94.7% of the original capacity (=24.8 mAh) was preserved after 20 cycles, confirming once again that each single-cell was well-prepared. The good cycling performance also implies that the internal resistances of the engaged single-cells are quite uniform, especially in the situation that no battery management systems are involved (Fig. 6d).

The single-cell textile battery was further tested in abnormal conditions including repeated folding-unfolding motions and high temperatures. Fig. 7a shows the voltage profile of the single-cell textile battery for 20 cycles. The interval of the folding-unfolding cycle was 310 s, and in each cycle, the textile battery was completely folded until the angles between the two sides of the folding edges became 180º and then stretched back to the original flat configuration. The repeated folding-unfolding motion was indeed reflected in the oscillation of the

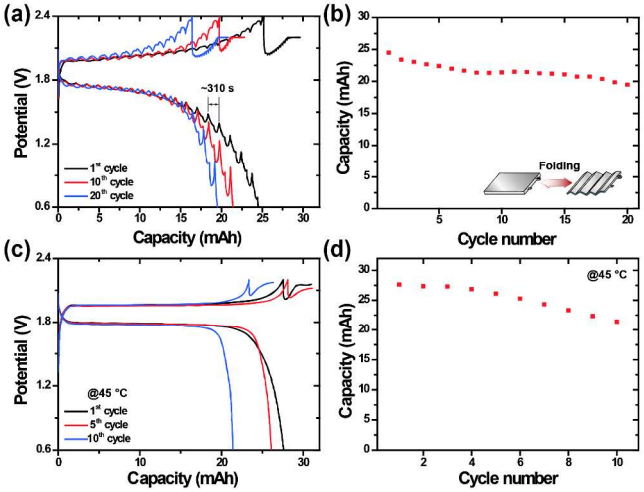

Fig. 7 Electrochemical characterization of the multi-stacked textile batteries during folding-unfolding motions. (a) Voltage profiles of the single-cell textile battery during folding-unfolding motions and (b) the corresponding cycle life. The folding motion is graphically illustrated in Fig. 3b inset. The C-rates for all of these results were 0.5C (=15.64 mA) for both charge and discharge in each cycle. (c) Voltage profiles of the single-cell textile battery and (d) its cycle life at 45 °C. The C-rates for all of these results were 0.5C (=14.91 mA) for both charge and discharge in each cycle.

voltage profiles with the same intervals. Even under such strong physical motions, the textile battery preserved 79.5% of the initial capacity (=24.5 mAh) after 20 cycles corresponding to 1,000 times folding-unfolding repetitions, suggesting that the cell holds remarkable mechanical stability by utilizing the internal fiber structure of the textile that releases the substantial stress efficiently while maintaining the adhesion of the electrode films (Fig. 7b). It should be noted that the degree of the folding in the current investigation was exaggerated, and actual folding/bending required for flexible batteries would be much more moderate. Also, for the outdoor and building applications, the textile battery should hold good electrochemical performance at high temperatures. To test such possibilities, the single-cells were evaluated at 45 ºC. As depicted in Fig. 7c, while the voltage profiles at 45 ºC exhibited almost the same voltages and plateaus as those at room temperature, the profiles at 45 ºC showed sharper voltage drops at the end of plateaus, which is attributed to increased ionic conductivity at the higher temperature[33]. At this temperature, the textile battery showed 77.5% retention after 10 cycles (Fig. 7d). The observed capacity drops might originate from unwanted side reactions with the Ni-coated textile that become amplified at high temperatures. (See Fig. S2†). This issue could be resolved by finding proper textiles or performing post-treatments, but we leave it as a future investigation.

Conclusions

In conclusion, we have demonstrated large area flexible LIBs with the multi-stack configuration. The mechanical stability of both single-cell and module levels during aggressive folding/bending motions originates from the use of the textile current collectors that release tensile/compressional stress efficiently through 3D porous structures. Moreover, a vast number of the possibilities in connecting the single-cells into modules represent additional opportunities in tuning the operation voltage and cell capacity. The present investigation suggests that flexible LIBs could find a broad range of unique applications beyond IT items once the cells are designed carefully from each component in a single-cell to module assembly.

Acknowledgements

We acknowledge the financial support by the National Research Foundation of Korea (NRF) grant funded by the Korea government (MEST) (NRF-2010-C1AAA001-0029031). This work also supported by the Technology Innovation Program funded by the Ministry of Trade, industry & Energy (MI, Korea) (MI-2013-10044519).

Notes and references

1. J. M. Tarascon and M. Armand, *Nature*, 2001, **414**, 359-367.
2. Y. Chen, J. Au, P. Kazlas, A. Ritenour, H. Gates and M. McCreary, *Nature*, 2003, **423**, 136-136.
3. M. Armand and J. M. Tarascon, *Nature*, 2008, **451**, 652-657.
4. J.-S. Kim, K. Kim, W. Cho, W. H. Shin, R. Kanno and J. W. Choi, *Nano Lett.*, 2012, **12**, 6358-6365.
5. Z. L. Wang and W. Wu, *Angew. Chem., Int. Ed.*, 2012, **51**, 11700-11721.
6. R. F. Service, *Science*, 2003, **301**, 909-911.
7. B. Scrosati, *Nat. Nanotechnol.*, 2007, **2**, 598-599.
8. H. Nishide and K. Oyaizu, *Science*, 2008, **319**, 737-738.
9. S. Xu, Y. Zhang, J. Cho, J. Lee, X. Huang, L. Jia, J. A. Fan, Y. Su, J. Su, H. Zhang, H. Cheng, B. Lu, C. Yu, C. Chuang, T.-i. Kim, T. Song, K. Shigeta, S. Kang, C. Dagdeviren, I. Petrov, P. V. Braun, Y. Huang, U. Paik and J. A. Rogers, *Nat. Commun.*, 2013, **4**, 1543.
10. W. Chen, R. B. Rakhi, L. Hu, X. Xie, Y. Cui and H. N. Alshareef, *Nano Lett.*, 2011, **11**, 5165-5172.
11. J. P. Rojas, G. A. Torres Sevilla and M. M. Hussain, *Sci. Rep.*, 2013, **3**.
12. G. Zhou, F. Li and H.-M. Cheng, *Energy Environ. Sci.*, 2014, DOI: 10.1039/C3EE43182G.
13. H. Gwon, J. Hong, H. Kim, D.-H. Seo, S. Jeon and K. Kang, *Energy Environ. Sci.*, 2014, **7**, 538-551.
14. Y. H. Kwon, S.-W. Woo, H.-R. Jung, H. K. Yu, K. Kim, B. H. Oh, S. Ahn, S.-Y. Lee, S.-W. Song, J. Cho, H.-C. Shin and J. Y. Kim, *Adv. Mater.*, 2012, **24**, 5192-5197.
15. S. Leijonmarck, A. Cornell, G. Lindbergh and L. Wagberg, *J. Mater. Chem. A*, 2013, **1**, 4671-4677.
16. S.-Y. Lee, K.-H. Choi, W.-S. Choi, Y. H. Kwon, H.-R. Jung, H.-C. Shin and J. Y. Kim, *Energy Environ. Sci.*, 2013, **6**, 2414-2423.

17. V. L. Pushparaj, M. M. Shaijumon, A. Kumar, S. Murugesan, L. Ci, R. Vajtai, R. J. Linhardt, O. Nalamasu and P. M. Ajayan, *Proc. Natl. Acad. Sci. U.S.A.*, 2007, **104**, 13574-13577.
18. L. Hu, J. W. Choi, Y. Yang, S. Jeong, F. La Mantia, L.-F. Cui and Y. Cui, *Proc. Natl. Acad. Sci. U.S.A.*, 2009.
19. Q. Cheng, Z. Song, T. Ma, B. B. Smith, R. Tang, H. Yu, H. Jiang and C. K. Chan, *Nano Lett.*, 2013, **13**, 4969-4974.
20. L. Hu, M. Pasta, F. L. Mantia, L. Cui, S. Jeong, H. D. Deshazer, J. W. Choi, S. M. Han and Y. Cui, *Nano Lett.*, 2010, **10**, 708-714.
21. L. Hu, F. La Mantia, H. Wu, X. Xie, J. McDonough, M. Pasta and Y. Cui, *Adv. Energy Mater.*, 2011, **1**, 1012-1017.
22. K. Jost, C. R. Perez, J. K. McDonough, V. Presser, M. Heon, G. Dion and Y. Gogotsi, *Energy Environ. Sci.*, 2011, **4**, 5060-5067.
23. K. Wang, P. Zhao, X. Zhou, H. Wu and Z. Wei, *J. Mater. Chem.*, 2011, **21**, 16373-16378.
24. K. Fu, O. Yildiz, H. Bhanushali, Y. Wang, K. Stano, L. Xue, X. Zhang and P. D. Bradford, *Adv. Mater.*, 2013, **25**, 5109-5114.
25. Z. Weng, Y. Su, D.-W. Wang, F. Li, J. Du and H.-M. Cheng, *Adv. Energy Mater.*, 2011, **1**, 917-922.
26. Y.-R. Kang, Y.-L. Li, F. Hou, Y.-Y. Wen and D. Su, *Nanoscale*, 2012, **4**, 3248-3253.
27. Y.-H. Lee, J.-S. Kim, J. Noh, I. Lee, H. J. Kim, S. Choi, J. Seo, S. Jeon, T.-S. Kim, J.-Y. Lee and J. W. Choi, *Nano Lett.*, 2013, **13**, 5753-5761.
28. H.-J. Ha, E.-H. Kil, Y. H. Kwon, J. Y. Kim, C. K. Lee and S.-Y. Lee, *Energy Environ. Sci.*, 2012, **5**, 6491-6499.
29. E.-H. Kil, K.-H. Choi, H.-J. Ha, S. Xu, J. A. Rogers, M. R. Kim, Y.-G. Lee, K. M. Kim, K. Y. Cho and S.-Y. Lee, *Adv. Mater.*, 2013, **25**, 1395-1400.
30. H. Gwon, H.-S. Kim, K. U. Lee, D.-H. Seo, Y. C. Park, Y.-S. Lee, B. T. Ahn and K. Kang, *Energy Environ. Sci.*, 2011, **4**, 1277-1283.
31. N. Li, Z. Chen, W. Ren, F. Li and H.-M. Cheng, *Proc. Natl. Acad. Sci. U.S.A.*, 2012, **109**, 17360-17365.
32. H. Y. Jung, M. B. Karimi, M. G. Hahm, P. M. Ajayan and Y. J. Jung, *Sci. Rep.*, 2012, **2**.
33. F. Croce, G. B. Appetecchi, L. Persi and B. Scrosati, *Nature*, 1998, **394**, 456-458.

Graphical Abstract

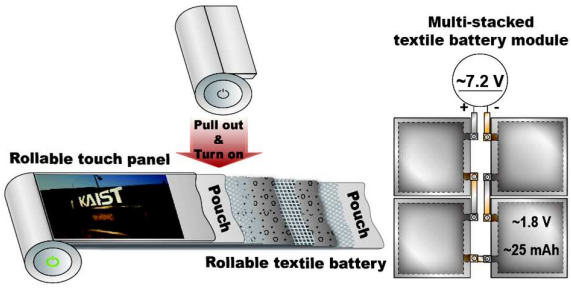

Large area multi-stacked lithium-ion battery modules are developed for flexible and rollable applications by employing conductive textiles.